AIAA JOURNAL
Vol. 43, No. 10, October 2005

Formation Criterion for Synthetic Jets

Ryan Holman* and Yogen Utturkar*
University of Florida, Gainesville, Florida 32611-6250
Rajat Mittal†
George Washington University, Washington, D.C. 20052
Barton L. Smith‡
Utah State University, Logan, Utah 84322
and
Louis Cattafesta§
University of Florida, Gainesville, Florida 32611-6250

A formation criterion for synthetic jets is proposed and validated. A synthetic jet actuator is a zero-net mass-flux device that imparts momentum to its surroundings. *Jet formation* is defined as the appearance of a time-averaged outward velocity along the jet axis and corresponds to the generation and subsequent convection or escape of a vortex ring. It is shown that over a wide range of operating conditions synthetic jet formation is governed by the jet Strouhal number *Sr* (or Reynolds number *Re* and Stokes number *S*). Both numerical simulations and experiments are performed to supplement available two-dimensional and axisymmetric synthetic jet formation data in the literature. The data support the jet formation criterion $1/Sr = Re/S^2 > K$, where the constant *K* is approximately 1 and 0.16 for two-dimensional and axisymmetric synthetic jets, respectively. In addition, the dependence of the constant *K* on the normalized radius of curvature of a rounded orifice or slot is addressed. The criterion is expected to serve as a useful design guide for synthetic jet formation in flow control, heat transfer, and acoustic liner applications, in which a stronger jet is synonymous with increased momentum transfer, vorticity generation, and acoustic nonlinearities.

I. Introduction

SYNTHETIC jet actuators are useful for thermal-fluid control applications, including mixing enhancement,[1] separation control,[2–4] thrust vectoring,[5] and heat transfer.[6–9] Figure 1 shows a schematic of a typical synthetic jet or zero-net mass-flux (ZNMF) actuator. In one implementation, a piezoelectric disk is bonded to a metal diaphragm, which is sealed to form a cavity having an orifice or slot. The cavity and orifice/slot form a Helmholtz resonator. As the diaphragm or driver oscillates, fluid is periodically entrained into and expelled from the orifice. During the expulsion portion of the cycle, a vortex ring can form near the orifice and, under certain operating conditions, convect away from the orifice to form a time-averaged jet. This behavior is defined as jet formation and was observed more than 50 years ago.[10] For other operating conditions, the vortex ring is ingested back into the slot during the suction part of the cycle, and no jet is formed.[11] When this occurs, it can seriously hamper heat-transfer enhancement in applications where the impinging vortices are used to cool electronic components. As will be shown later in the paper, jet formation is directly related to the flux of vorticity from the synthetic jet. Because vorticity flux is a quantity that is quite important in applications where jets operate in a crossflow,[12] it is clear that understanding jet formation in quiescent flow is a crucial first step towards understanding their performance vis à vis vorticity flux in these crossflow applications. Jet formation also leads to the generation of nonlinear resistance effects in Helmholtz resonators used in acoustic liners, which complicates their modeling and design.[10,13,14] Thus, the development of a simple jet formation criterion will be quite useful for such applications and is the primary objective of this paper.

The governing parameters for a synthetic jet based on a simple "slug-velocity-profile" model include a dimensionless stroke length L_0/d and a Reynolds number $Re_{U_0} = U_0 d/\nu$ based on the velocity scale

$$U_0 = fL_0 = f\int_0^{T/2} u_0(t)\,\mathrm{d}t \tag{1}$$

where d is the diameter of the orifice (or the width of the slot), ν is the kinematic viscosity of the fluid, $u_0(t)$ is the centerline velocity at the exit, $T = 1/f$ is the period, f is the frequency of oscillation, and L_0 is the distance that a slug of fluid travels away from the orifice during the ejection portion of the cycle or period.[15–17] Later, Smith and Swift[18] argued that because the spatial velocity profile can deviate significantly from the assumed slug shape the centerline velocity profile $u_0(t)$ is more generally defined as the spatial-averaged velocity at the exit.

Alternatively, a jet Reynolds number can be defined in terms of an average jet velocity during the expulsion stroke[19]:

$$Re_{\bar{U}} = \bar{U}d/\nu \tag{2}$$

where $\bar{U}$ is the time- and spatial-averaged exit velocity

$$\bar{U} = \frac{2}{T}\frac{1}{A}\int_A\int_0^{T/2} u(t, y)\,\mathrm{d}t\,\mathrm{d}A \tag{3}$$

Here, A is the orifice exit area, and y is the cross-stream coordinate (see Fig. 1). Equations (1) and (3) reveal that the two velocity scales are related by $\bar{U} = 2U_0$.

Furthermore, note that $L_0/d = U_0/(fd)$ is closely related to the inverse of the Strouhal number via

$$1/Sr = (L_0/d)/\pi = \bar{U}/\omega d = (\bar{U}d/\nu)/(\omega d^2/\nu) = Re/S^2 \tag{4}$$

Received 9 July 2004; revision received 23 March 2005; accepted for publication 3 June 2005.

*Graduate Research Assistant, Department of Mechanical and Aerospace Engineering. Student Member AIAA.
†Associate Professor, Mechanical and Aerospace Engineering Department. Senior Member AIAA.
‡Assistant Professor, Mechanical and Aerospace Engineering Department. Member AIAA.
§Associate Professor, Department of Mechanical and Aerospace Engineering; cattafes@ufl.edu. Associate Fellow AIAA.

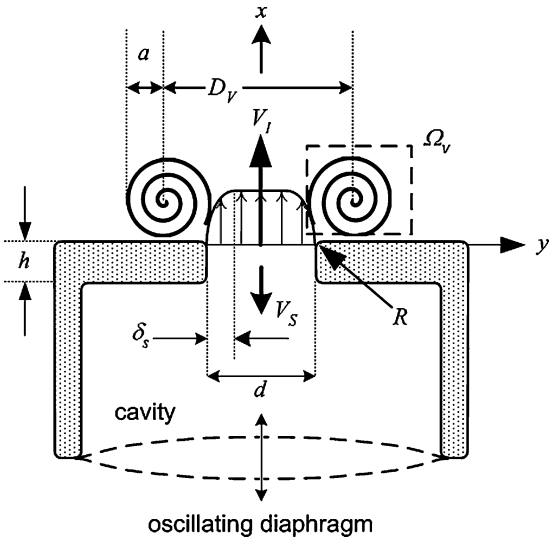

Fig. 1 Schematic of a synthetic jet.

where S is the Stokes number given by

$$S = \sqrt{\omega d^2/\nu} \tag{5}$$

and $\omega = 2\pi f$ is the radian frequency of oscillation. The ability of a ZNMF actuator to impart momentum to its surroundings is highly dependent on these nondimensional numbers and, in addition, on the slot/orifice geometry.[19,20]

The purpose of this paper is to propose and validate a unified jet formation criterion suitable for circular orifices and rectangular slots with a radius of curvature. First, a jet formation criterion based on a simple order-of-magnitude analysis is presented. Next, computational and experimental flow-visualization experiments are described to determine the onset of vortex escape (i.e., jet formation). Detailed flow measurements are used to determine the jet formation parameters. Finally, available data are used to validate the criterion.

II. Vortex-Based Jet Formation Criterion

Smith and Swift[18] and Rampunggoon[11] independently proposed a jet formation criterion for two-dimensional synthetic jets. Smith and Swift[18] argued that a threshold stroke length L_0/d exists for jet formation. On the other hand, Rampunggoon[11] used a simple order-of-magnitude analysis to show that the ratio of the Reynolds number to the square of the Stokes number must be greater than some constant to ensure jet formation. Preliminary computational and experimental validations of this criterion were subsequently accomplished by Utturkar[19] and Utturkar et al.,[21] respectively. The order-of-magnitude analysis is summarized next.

Figure 1 illustrates a vortex ring emanating from a slot (or orifice). The ability of the ring to overcome the suction velocity during the ingestion stroke depends on its self-induced velocity, which in turn is a function of the vortex strength. The strength of each shed vortex Ω_v has been shown by Didden[22] to be related to the flux of vorticity through a (x, y) planar slice of the half-slot during the ejection phase of the cycle

$$\Omega_v = \int_0^{T/2} \int_0^{d/2} \xi_z(y,t)u(y,t)\,\mathrm{d}y\,\mathrm{d}t \tag{6}$$

where $\xi_z(y,t)$ is the spanwise (or azimuthal) vorticity component at the exit for a two-dimensional (or axisymmetric) case and $u(y,t)$ is the exit jet x velocity. In Fig. 1, δ_s is the size of the shear flow region characterized by nonzero vorticity. The induced velocity of the dipole V_I is thus proportional to Ω_v/d, where d is the slot width. An order-of-magnitude analysis of Eq. (6) results in

$$\Omega_v \sim (\bar{U}/\delta_s)\bar{U}\delta_s(1/\omega) \sim \bar{U}^2/\omega \tag{7}$$

If it is assumed that a jet will form when the induced velocity of the dipole V_I is somewhat larger than the average jet suction velocity $V_s \sim \bar{U}$, it follows that the ratio of the induced dipole velocity to the suction velocity is

$$V_I/V_s \sim (\Omega_v/d)/\bar{U} \sim \bar{U}/\omega d = 1/Sr$$
$$= (\bar{U}d/\nu)/(\omega d^2/\nu) = Re/S^2 > K \tag{8}$$

where K is an $\mathcal{O}(1)$ constant.

Equation (8) states that a vortex escapes or a jet is formed when the Strouhal number is below a critical value. We now seek to perform a dimensional analysis of the synthetic jet problem using the Buckingham–Pi theorem to bolster this argument. The dependent parameter is the average jet velocity $\bar{U}$ and is a function of the geometry of the device, the diaphragm, and fluid properties. The geometric properties of the two-dimensional synthetic jet include the slot width d, the neck height h, the slot depth in the spanwise direction w, the radius of curvature of the slot edge R, and the volume of the synthetic jet cavity $\forall$. It has been previously shown that the behavior of the flowfield emanating from the slot is primarily sensitive to the cavity volume and not its shape.[23] The oscillatory diaphragm properties include the angular frequency of oscillation ω, its fundamental resonant frequency ω_d, and the volume displaced by it $\Delta\forall$, whereas the relevant fluid properties are the isentropic speed of sound c_0 and the kinematic viscosity ν. These 11 parameters contain the two primary dimensions of length and time; thus, there are 9 dimensionless parameters. Choosing the slot width d and the actuator frequency ω as repeating parameters, the following groups are obtained:

$$\bar{U}/\omega d = f\left(\forall/d^3, h/d, w/d, R/d, \omega_d/\omega, \Delta\forall/d^3, c_0/\omega d, \nu/\omega d^2\right) \tag{9}$$

Equation (9) can be rearranged by recombining the pi groups as

$$Sr = f\left(\omega/\omega_H, h/d, w/d, \varepsilon, \omega/\omega_d, \Delta\forall/d^3, kd, S\right) \tag{10}$$

where Sr is the Strouhal number; ω/ω_H is the ratio of the oscillation frequency to the Helmholtz frequency of the device $\omega_H \simeq c_0\sqrt{(wd/\forall h)}$, which is a measure of the compressibility of the flow in the cavity; h/d is the slot height aspect ratio; w/d is the slot depth aspect ratio; $\varepsilon = 2R/d$ is the normalized radius of curvature of the slot; ω/ω_d is the ratio of the oscillation frequency to the resonant frequency of the diaphragm; $\Delta\forall/d^3$ is the ratio of the displaced cavity volume to the cube of the slot width; kd is the dimensionless wave number; and S is the Stokes number as defined earlier. For a given fluid (i.e., ideal gas), diaphragm, and actuator geometry, the Strouhal number will only change because of variations in the following parameters:

$$Sr = f\left(\omega/\omega_H, \omega/\omega_d, \Delta\forall/d^3, kd, S\right) \tag{11}$$

If the frequency of oscillation is also fixed, then Eq. (11) reduces to

$$Sr = f(\Delta\forall/d^3) \tag{12}$$

Thus, for a given ZNMF device operating at a fixed frequency, the dimensionless diaphragm amplitude controls the Strouhal number. From Eq. (8), the Strouhal number will decrease as $\Delta\forall/d^3$ increases, eventually forming a jet.

Of course, based on the preceding dimensional analysis, we expect that the value of the constant K in Eq. (8) will be affected by the orifice geometry, namely, the aspect ratio h/d and the exit edge shape (sharp or rounded, etc.). The constant is also expected to assume different values for two-dimensional and axisymmetric models having similar orifice geometry because of different functional forms of solutions to fully developed unsteady pressure-driven flow in a pipe vs a two-dimensional channel.[24] Although the focal point in this paper is on the jet formation criterion and its validation, the influence of the aforesaid factors on the scaling constant is recognized and briefly discussed next.

A. Effect of Orifice Geometry

The influence of the orifice geometry on the value of the constant K can be reasonably explained by a simple extension to the preceding scaling. Equation (6) can be adapted for a jet with a rounded

edge to

$$\Omega_v = \int_0^{T/2} \int_0^{d/2+R} \frac{-\partial u(y,t)}{\partial y} u(y,t)\,\mathrm{d}y\,\mathrm{d}t \tag{13}$$

where R is the radius of curvature (see Fig. 1). The no-slip boundary condition for $u(y,t)$ is $u(d/2+R,t)=0$. Exact integration of Eq. (13) yields

$$\Omega_v = \int_0^{\pi/\omega} \frac{1}{2} u(0,t)^2\,\mathrm{d}t \tag{14}$$

which can be evaluated by assuming a sinusoidal form of the centerline velocity $u(0,t) = U_{\mathrm{cl}} \sin(\omega t + \phi)$.

$$\Omega_v = \tfrac{1}{4}(\pi/\omega) U_{\mathrm{cl}}^2 \tag{15}$$

Equation (15) shows that the resulting vorticity flux is a function of the centerline velocity and frequency. By analogy with steady pressure-driven flow in a channel or pipe, we will define the ratio of the amplitude of the spatial-averaged velocity U_{avg} to the amplitude of the centerline velocity U_{cl} as a frequency-dependent constant $U_{\mathrm{avg}}/U_{\mathrm{cl}} = c$. Next, from Eq. (3) $\bar{U} = 2U_{\mathrm{avg}}/\pi$, so that

$$\Omega_v = \tfrac{1}{4}(\pi/\omega)\left(U_{\mathrm{avg}}^2/c^2\right) = \tfrac{1}{4}(\pi/\omega)[(\pi\bar{U}/2)^2/c^2] \tag{16}$$

Employing the nondimensional exit radius of curvature defined earlier, $\varepsilon = 2R/d$, the following heuristic expression[25,26] can be employed to estimate the induced velocity:

$$V_I = \kappa(\Omega_v/2\pi D_V) = \kappa\left[\Omega_v/2\pi d(1+\varepsilon)^p\right] \tag{17}$$

by modeling the distance between the vortex centers (D_V in Fig. 1) as equal to $d(1+\varepsilon)^p$. Here, the exponent $p<1$ accounts grossly for flow separation caused by the exit curvature, and κ is a constant that depends on the ratio of the vortex core radius a to the distance between the two vortex centers D_V (see Fig. 1). Substituting Eq. (16) into Eq. (17) and then this result into Eq. (8) results in a general jet formation criterion

$$\frac{1}{Sr} = \frac{Re}{S^2} > \underbrace{\frac{32c^2(1+\varepsilon)^p}{\kappa\pi^2}}_{\text{jet formation constant}} \tag{18}$$

First, Eq. (18) indicates a smaller jet formation constant for orifices with a sharp exit (small ε) as compared to those with a finite radius of curvature ε. In other words, a fillet radius will tend to delay the formation of discrete vortices (although this does not imply anything about the efficiency of jet formation[20]). Second, the constant is directly proportional to the square of $c = U_{\mathrm{avg}}/U_{\mathrm{cl}} \le 1$, which is, in turn, affected by the geometry of the orifice and the Stokes number.[24] Furthermore, the constant is proportional to $1/\kappa$, where κ in Eq. (17) depends on whether a vortex dipole (in the case of a slot) or ring (in the case of an orifice) is considered.[25,26] The distinction between a rectangular slot and an axisymmetric circular orifice is discussed further next.

B. Two-Dimensional vs Axisymmetric Jet

Past studies[25,26] have estimated the constant κ in Eq. (17) as a function of a/D_V in the case of two-dimensional vortex dipoles and axisymmetric vortex rings. For $0 < a/D_V < 0.5$, the value of κ in the two-dimensional case lies between 20–40% of that for the axisymmetric case. Furthermore, the constant $c = U_{\mathrm{avg}}/U_{\mathrm{cl}}$ assumes a different value for the two-dimensional and axisymmetric cases. For example, for a fully developed, laminar, steady flow, the velocity profile shape is parabolic, and c is 0.67 and 0.5 for two-dimensional and axisymmetric flow, respectively. For large S, the value of c tends to 1 (a slug profile) for both cases. Consequently, these combined effects suggest that the formation constant for axisymmetric jets is significantly lower, by up to almost an order of magnitude, than its two-dimensional counterpart. This is validated by numerical simulations and experiments described next.

III. Computational Studies

Numerical simulations are performed to characterize a two-dimensional synthetic jet. A previously developed and extensively validated Cartesian grid solver[27–29] is employed in these simulations to facilitate simulation of unsteady viscous incompressible flows with complex immersed moving boundaries on Cartesian grids. The solver employs a second-order-accurate central difference scheme for spatial discretization and a mixed explicit-implicit fractional step scheme for time advancement, which is also second-order accurate. An efficient multigrid algorithm is used for solving the pressure Poisson equation. The second-order spatial accuracy of the code has been clearly demonstrated[27,28] along with validation for a number of canonical flow cases. Furthermore, the code has also been validated against experiments by simulating a transitional jet in quiescent flow.[30]

The key advantage of this solver for the current problem is that the entire geometry of the actuator including the oscillating diaphragm is modeled on a stationary Cartesian mesh. As the diaphragm moves over the underlying Cartesian mesh, the discretization in the cells cut by the solid boundary is modified to account for the presence of the solid boundary. In addition, a soft velocity boundary condition, which accommodates the jet flow, is applied on free boundaries. All simulations are run until initial transients decay and statistics are accumulated beyond this over a number of cycles. The exit curvature for all computed cases amounts to $\varepsilon = 0.15$. A dense 600×220 grid is employed for these simulations. The grid has been carefully designed so as to provide adequate resolution to the key features of the flowfield while minimizing spurious numerical effects. For instance, we use uniform meshes in and around the jet slot and provide a relatively high resolution to the boundary layers that develop on the slot walls as well as the vortices that form at the lips of the slots. In the external flow, the mesh is slowly stretched in the vertical direction in a way that corresponds roughly with the increasing size of the eddies in the synthetic jet. A large external domain size of over 30 slot widths in each direction is chosen so as to minimize the effect of the external boundary on the computed flow near the slot. The grid has been chosen after extensive grid and domain sensitivity studies, which are reported in Mittal and Rampunggoon.[31] The computations also employ about 2000 time steps per cycle, which leads to very high temporal resolution of the flow.

Figure 2a shows a simulation result at two phases in a cycle for a case with no jet formation. For this case, $Re/S^2 = 0.76$. As illustrated in Fig. 2a, the vortices formed at the orifice during the

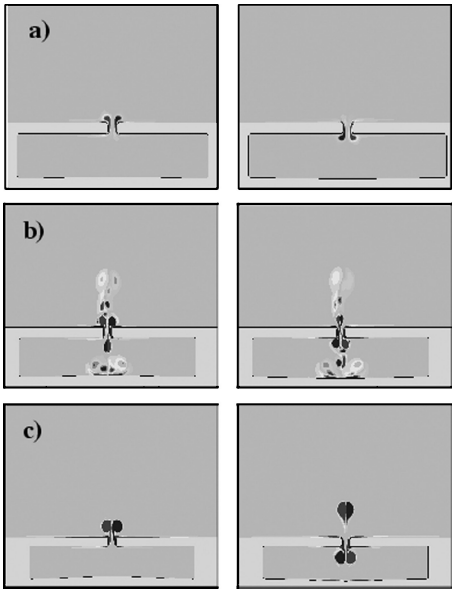

Fig. 2 Vorticity plots from two-dimensional synthetic jet simulations indicating the dynamics of the vortex dipole between minimum and maximum cavity volume stages respectively $S = 15.8$: a) no jet ($Re/S^2 = 0.76$), b) transition ($Re/S^2 = 1.02$), and c) jet ($Re/S^2 = 1.92$).

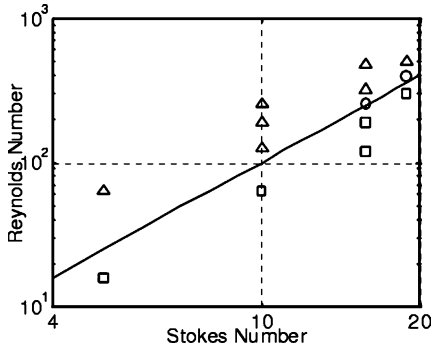

Fig. 3 Summary of observations made regarding jet formation from two-dimensional synthetic jet computations: ——, $Re/S^2 = 1$; □, no jet; ○, transition; and △, clear jet.

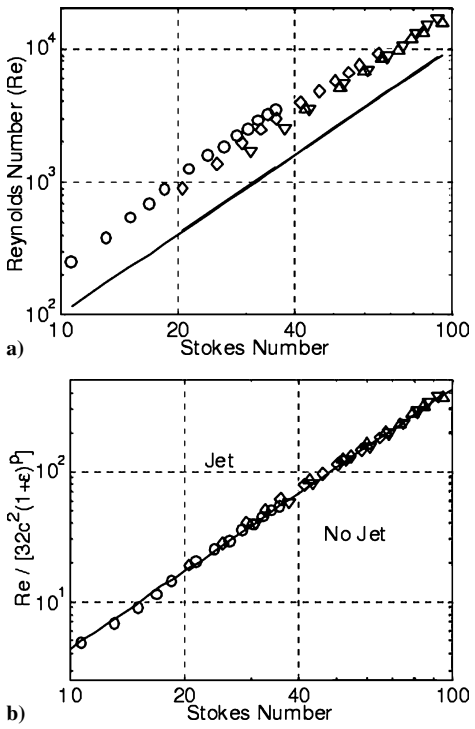

Fig. 4 Jet formation threshold for two-dimensional synthetic jets: a) experimental data of Smith and Swift,[18] ——, $Re/S^2 = 1$; b) normalized data of Smith and Swift to account for Stokes number and radius of curvature, ——, $\{Re/[32c^2(1+\varepsilon)^p]\}/S^2 = 0.0425$. Data points denote threshold value for clear jet formation: ○, $\varepsilon = 2.4$; ◇, $\varepsilon = 1.2$; ▽, $\varepsilon = 0.84$; and △, $\varepsilon = 0.61$.

expulsion part of the cycle are reingested during the suction part. Figure 2b shows a transitional case with $Re/S^2 = 1.02$ in which jet formation is not readily apparent. Figure 2c corresponds to a case with $Re/S^2 = 1.92$ and is an example of a case exhibiting a clear jet formation as indicated by the expelled vortex ring. A series of numerical simulations over a range of Reynolds and Stokes numbers suggest that the constant $K > \mathcal{O}(1)$, as shown in Fig. 3.

IV. Experimental Studies

The data of Smith and Swift[18] are recast to yield Reynolds and Stokes numbers and are presented in Fig. 4a. Their ZNMF device consists of a speaker-driven diaphragm and a two-dimensional slot with an aspect ratio h/d much greater than one (i.e., $12 < h/d < 47$). The jet formation threshold was determined by increasing the driver amplitude until a jet was detected visually. Clearly, a general trend of the jet formation criterion $Re/S^2 >$ constant is observed for the experimental results, which correspond to clear jet formation. The normalized radius of curvature ε varies considerably in their experiments. A closer look at Fig. 4a, however, verifies Eq. (18), namely, that a jet is more easily formed for a sharp-edged slot, which is consistent with the discussion in Sec. II.A.

Table 1 ZNMF actuator details

Property	Value
Cavity volume, m^3	5.50×10^{-6}
Orifice diameter, mm	2.00
Orifice thickness, mm	1.65

Table 2 PIV measurement details

Property	Value
CCD camera lens[a]	200-mm micro with bellows extender
CCD camera image size, pixels	1024×1024
Spatial resolution, μm/pixel	7.7
Interrogation window size, pixels	32×32
Time ΔT between captures, μs	15–250
Number of image pairs	270–360
Phase resolution, deg	1.00–1.33
Velocity vector overlap, %	50
Measurement location, x/d	0.08
Number of velocity vectors across orifice	15

[a]CCD = charge-coupled device.

By comparison, in Fig. 4b we seek to minimize the combined influence of exit curvature and Stokes number on the data (via $c = U_{\text{avg}}/U_{\text{cl}}$) by normalizing the Reynolds number by the constant $32c^2(1+\varepsilon)^p$, as derived in Eq. (18). This normalization of the Reynolds number attempts to unify the jet formation analysis for synthetic jets with varying exit curvature and operating over a wide range of Stokes numbers. The exit plane velocity profile, as a function of S, is modeled by the unsteady flow solution for a fully developed channel flow subject to an oscillatory pressure gradient.[24,32] Although the exit plane velocity profile can tend to deviate from the assumed channel flow solution because of entrance effects, the preceding assumption does not produce any noticeable discrepancy in the scaling analysis, as seen from Fig. 4b. The value of c is numerically estimated by an integral analysis of the velocity profile. The exponent $p = 0.62$ provides the best qualitative agreement within the wide-ranging experimental data, as depicted in Fig. 4b. Despite the apparent agreement, the analysis in Sec. II.A is inadequate to precisely model all complexities of the flow in the jet orifice and only serves to estimate the impact of the significant factors on the scaling constant. In particular, there is insufficient information at present to calculate the constant κ in Eq. (18) because of a lack of knowledge of the vortex size and spacing.

Experimental jet formation data for the axisymmetric case were published over 50 years ago by Ingard and Labate.[10] More recent studies[33,34] suggest that $L_0/d > 1$ for axisymmetric jet formation. However, the range of Stokes numbers covered by these studies is high: $S > 35$. An extension to the low-Stokes-number range is desired and would prove useful in applications involving large-scale flow control experiments and engine nacelle acoustic liners.[35] Therefore, an axisymmetric ZNMF actuator is constructed to operate at a low-Stokes-number range: $6 \leq S \leq 36$. The construction of the cavity and the piezoelectric diaphragm is nearly similar to case 2 described in Gallas et al.,[36] and the geometric parameters of the ZNMF actuator are given in Table 1.

Particle-image-velocimetry (PIV)-based flow visualization is first used to determine the onset of jet formation, and Table 2 summarizes the parameters pertaining to the PIV setup. Successive images are acquired at a frame rate that is slightly different than a submultiple of the actuation frequency (similar to the schlieren imaging of Smith and Glezer[16]). Thus a different vortex ring is captured in each image at a slightly different phase in the cycle. The resulting sequence of images then forms an "aliased movie" of the flowfield. Velocity vector fields over one aliased cycle of the synthetic jet are acquired, and vorticity contours are computed for each frame. The resulting aliased movie of the vortex escape is then used to determine jet

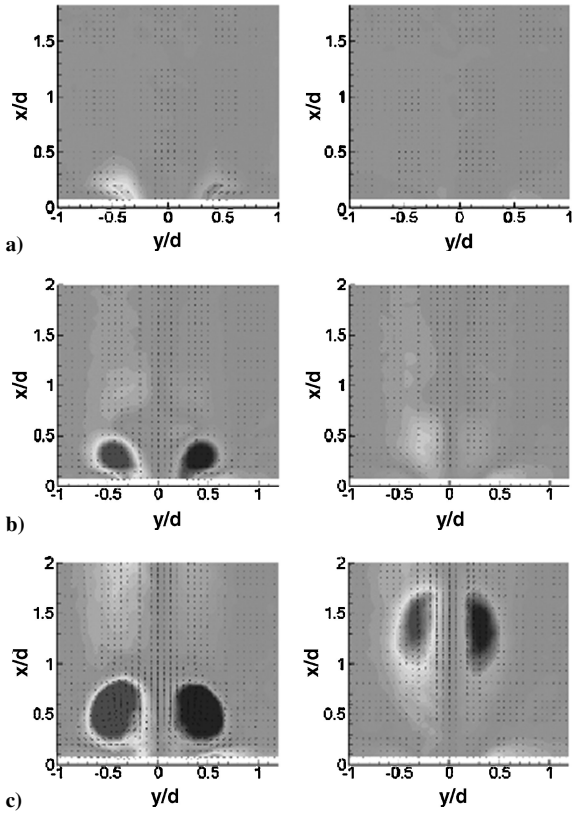

Fig. 5 PIV velocity vector fields with overlaid vorticity contours for minimum and maximum cavity volume stages respectively, $S = 18$ circular orifice: a) no jet ($Re/S^2 = 0.14$), b) transition ($Re/S^2 = 0.25$), and c) jet ($Re/S^2 = 0.37$).

formation. Figure 5 shows the evolution of vorticity during the minimum and maximum cavity volume stages of the cycle for $S = 18$ under no-jet, transitional, and clear-jet formation conditions, respectively. These images for the axisymmetric case are in good qualitative agreement with their two-dimensional simulation counterparts in Fig. 2. The mean flow from the orifice is presented in Fig. 6 for the corresponding cases in Fig. 5. Indeed, the formation of a mean jet, evident in Fig. 6c, corresponds to the case of vortex escape in Fig. 5c.

In contrast with the Stokes number, estimating the jet Reynolds number is difficult because the average volume flow rate during the expulsion part of the cycle $\bar{Q}$, and hence $\bar{U}$ from Eq. (3), must be determined by measuring the phase-locked, spatially varying velocity profile across the surface of the orifice. Given the small diameter of the orifice, the accuracy of the PIV-computed velocity profiles was deemed questionable. In addition, the spatial resolution of the PIV data was 246 μm, and the depth of field and light sheet thickness were approximately 0.25 and 0.15 mm, respectively. Furthermore, a relatively small number of images were acquired. Thus, laser Doppler anemometry (LDA) was used to measure phase-locked velocity profiles of select cases to validate the PIV results. The principle advantage of using LDA with 90-deg off-axis receiving optics vs PIV to measure velocity is the potential to achieve a much higher spatial resolution. Using the same 200-mm microlens with bellows extension as the PIV system in an off-axis receiving optics configuration that uses a pinhole aperture, the LDA probe volume is approximately $(0.058\ \text{mm})^3$, giving a spatial resolution approximately four times better than the present PIV setup. Phase-averaged velocity measurements are acquired at a given point with a resolution of 10 deg, and approximately 100 velocity values are acquired at each phase angle.

Once the velocity profiles at the surface of the orifice are acquired, whether using PIV or LDA, the profiles are spatially integrated to determine the volume flow rate as a function of phase angle. The locus of the positive values of the volume flow rate is then integrated to give the time-averaged volume flow rate during the expulsion

Table 3 Comparison between PIV- and LDA-acquired Reynolds numbers

Measurement technique and location	$S = 12$, no-jet formation	$S = 18$, clear-jet formation
PIV, $x/d = 0.08$	$17.8 \pm 3\%$	$121.2 \pm 3.7\%$
LDA, $x/d = 0.08$	$18.9 \pm 3\%$	$121.4 \pm 3\%$
LDA, $x/d = 0.03$	$18.1 \pm 3\%$	$126.9 \pm 3\%$

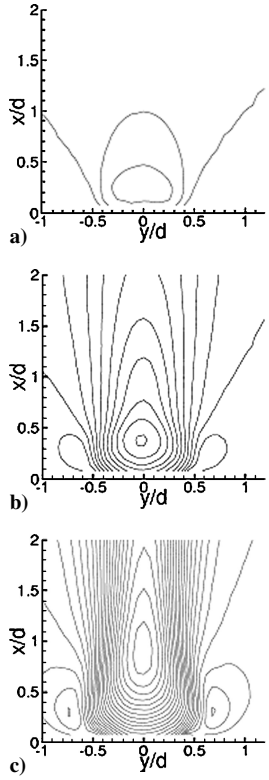

Fig. 6 U-component velocity contours corresponding to Fig. 5, increment between contour lines is 0.05 m/s, $S = 18$, circular orifice: a) no jet ($Re/S^2 = 0.14$), b) transition ($Re/S^2 = 0.25$), and c) jet ($Re/S^2 = 0.37$).

part of the cycle $\bar{Q}$, which is related to the average velocity by $\bar{Q} = \bar{U}\pi d^2/4$. Thus, the Reynolds number as defined in Eq. (2) can be recast as

$$Re_{\bar{U}} = 4\bar{Q}/\pi \nu d \tag{19}$$

Because of the previously mentioned limitations of the PIV system, the closest plane at which velocity data can be obtained is at $x/d = 0.08$, and fluid entrainment at this location can be nonnegligible. Therefore, velocity profiles are acquired closer to the surface of the orifice ($x/d = 0.03$) using LDA. The computed Reynolds numbers are compared with their uncertainty estimates using the two different methods. Table 3 summarizes the comparison between the computed Reynolds number using PIV and LDA, for two different Stokes-number cases. The data agree to within the 95% confidence intervals for all cases. Thus, we conclude that the PIV-computed Reynolds numbers at $x/d = 0.08$ are sufficiently accurate for the purposes of determining a jet formation criterion.

The jet formation data from the current experiments along with the axisymmetric data from Ingard and Labate[10] and Smith et al.[33] are compared in Fig. 7. It is found that the available data are consistent with the jet formation criterion with an empirically determined constant K equal to approximately 0.16.

The deviation of Ingard and Labate's data at their four lowest Reynolds numbers is interesting. Ingard and Labate report "particle-velocity" measurements but do not provide any description of the method or uncertainty in the data. In a later paper, however, Ingard[37] clarified these data as rms velocities obtained from a hot-wire anemometer. These four points correspond to very low particle velocities in the range of 10–60 cm/s. Thus, these data are deemed

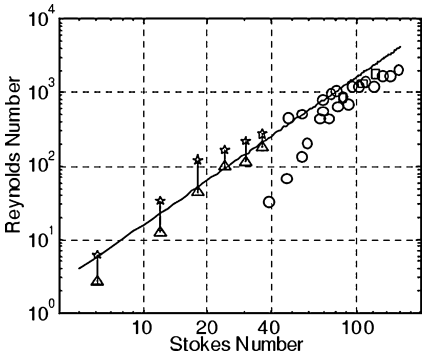

Fig. 7 Jet formation criterion for axisymmetric case: ——, Re/S^2 = 0.16; ○, threshold jet formation values of Ingard and Labate[10]; □, threshold jet formation values of Smith et al.[33]; △, maximum values of no jet formation acquired for the current study; and ★, minimum values of observed jet formation acquired for the current study.

questionable because of free-convection effects and the strong fluctuating component compared to the near-zero mean value.

V. Conclusions

A formation criterion for both two-dimensional and axisymmetric synthetic jets has been presented and evaluated. Jet formation depends on the dimensionless stroke length (i.e., Strouhal number) or, alternatively, the Reynolds number and Stokes number. The available data in the literature have been supplemented with current computational and experimental data. All of the data are consistent with the proposed jet formation criterion that $1/Sr = Re/S^2 > K$, where the constant K is dependent upon geometric factors such as orifice/slot shape, radius of curvature, and aspect ratio of the slot. Because cavity compressibility can be significant and the velocity profile can deviate from being slug like, computing the stroke length of the oscillating diaphragm in the cavity and applying continuity at the orifice, although appealing, is insufficient to determine Reynolds number in the general case of a compressible fluid (i.e., air) and a nonrigid diaphragm (e.g., a piezoelectric diaphragm). Instead, the more difficult task of measuring the exit velocity profile must be undertaken in order to accurately compute the Reynolds number. Alternatively, one can use a model, such as that proposed in Gallas et al.,[36] to predict the nominal exit velocity and determine if a jet is formed using the proposed criterion.

The jet formation criterion is expected to be useful for applications of synthetic jets, which rely on the successful formation or suppression of vortex rings ejected into quiescent fluid. For example, in a study investigating the application of synthetic jets for heat transfer to cool a laptop computer,[7] it was reported that a typical frequency of oscillation was 100 Hz and a typical orifice diameter was 1.6 mm. The Stokes number of this flow is approximately 10. Based on the current jet formation criterion, the Reynolds number should be of order 16 to form a jet, which translates to a minimum jet velocity of order 16 cm/s. The investigators reported a jet centerline velocity of 14 m/s at two orifice diameters downstream, which indicates the formation of a jet having significant strength.

The present criterion can be a significant asset to the design of flow-control actuators, where vortex escape and concomitant large vorticity and momentum injection is potentially required for good performance. Finally, it is expected that this criterion will aid in the modeling and subsequent design of acoustic liners, where vortex escape leads to complicating nonlinear effects.[10,13,14]

The present results are, however, insufficient to identify a universal jet formation constant. More detailed data concerning the separation, size, and trajectory of the expelled vortices are required for this purpose.

Acknowledgments

The University of Florida acknowledges support from Air Force Office of Scientific Research Grant F49620-03-1-0135, monitored by Tom Beutner. R. Mittal acknowledges support from NASA Grant NAG-1-01024 monitored by Susan Gorton. The authors gratefully acknowledge B. Carroll and M. Sheplak for their contributions to this paper.

References

[1]Chen, Y., Liang, S., Aung, K., Glezer, A., and Jagoda, J., "Enhanced Mixing in a Simulated Combustor Using Synthetic Jet Actuators," AIAA Paper 99-0449, Jan. 1999.

[2]Amitay, M., Kibens, V., Parekh, D., and Glezer, A., "The Dynamics of Flow Reattachment over a Thick Airfoil Controlled by Synthetic Jet Actuators," AIAA Paper 99-1001, Jan. 1999.

[3]Crook, A., Sadri, M., and Wood, N. J., "The Development and Implementation of Synthetic Jets for Control of Separated Flow," AIAA Paper 99-3176, June 1999.

[4]Seifert, A., and Pack, L. G., "Oscillatory Control of Separation at High Reynolds Numbers," *AIAA Journal*, Vol. 37, No. 9, 1999, pp. 1062–1071.

[5]Smith, B. L., and Glezer, A., "Jet Vectoring Using Synthetic Jets," *Journal of Fluid Mechanics*, Vol. 458, 2002, pp. 1–34.

[6]Beratlis, N., and Smith, M. K., "Optimization of Synthetic Jet Cooling for Microelectronics Applications," *Annual IEEE Semiconductor Thermal Measurement and Management Symposium*, Inst. of Electrical and Electronics Engineers, 2003, pp. 66–73.

[7]Campbell, J. S., Black, W. Z., Glezer, A., and Hartley, J. G., "Thermal Management of a Laptop Computer with Synthetic Air Microjets," *Sixth Intersociety Conference on Thermal and Thermomechanical Phenomenon in Electronic Systems*, Inst. of Electrical and Electronics Engineers, 1998, pp. 43–50.

[8]Mahalingam, R., and Glezer, A., "Air Cooled Heat Sinks Integrated with Synthetic Jets," *Thermomechanical Phenomena in Electronic Systems—Proceedings of the Intersociety Conference*, Inst. of Electrical and Electronics Engineers, 2002, pp. 285–291.

[9]Trávníček, Z., and Tesař, V., "Annular Synthetic Jet used for Impinging Flow Mass-Transfer," *International Journal of Heat and Mass Transfer,* Vol. 46, No. 17, 2003, pp. 3291–3297.

[10]Ingard, U., and Labate, S., "Acoustic Circulation Effects and the Nonlinear Impedance of Orifices," *Journal of the Acoustical Society of America*, Vol. 22, No. 2, 1950, pp. 211–218.

[11]Rampunggoon, P., "Interaction of a Synthetic Jet with a Flat Plate Boundary Layer," Ph.D. Dissertation, Dept. of Mechanical Engineering, Univ. of Florida, Gainesville, FL, Dec. 2001.

[12]Yehoshua, T., and Seifert, A., "Boundary Condition Effects on Oscillatory Momentum Generators," AIAA Paper 2003-3710, June 2003.

[13]Choudhari, M., Khorrami, M. D., and Edwards, J. R., "Computational Study of Micro Fluid Mechanics of Duct Acoustic Treatment," AIAA Paper 99-1851, May 1999.

[14]Tam, C. K. W., Ju, H., Jones, M. G., Watson, W. R., and Parrott, T. L., "A Computational and Experimental Study of Slit Resonators," AIAA Paper 2003-3310, May 2003.

[15]Glezer, A., and Amitay, M., "Synthetic Jets," *Annual Review of Fluid Mechanics*, Vol. 34, 2002, pp. 503–529.

[16]Smith, B., and Glezer, A., "The Formation and Evolution of Synthetic Jets," *Physics of Fluids*, Vol. 10, No. 9, 1998, pp. 2281–2297.

[17]Glezer, A., "The Formation of Vortex Rings," *Physics of Fluids*, Vol. 31, No. 12, 1988, pp. 3532–3542.

[18]Smith, B., and Swift, G., "Synthetic Jets at Large Reynolds Number and Comparison to Continuous Jets," AIAA Paper 2001-3030, June 2001.

[19]Utturkar, Y., "Numerical Investigation of Synthetic Jet Flow Fields," M.S. Thesis, Dept. of Mechanical Engineering, Univ. of Florida, Gainesville, FL, May 2002.

[20]Fugal, S. R., Smith, B. L., and Spall, R. E., "A Numerical Study of 2-D Synthetic Jet Formation," American Society of Mechanical Engineers, Paper HT-FED2004-56854, July 2004.

[21]Utturkar, Y., Holman, R., Mittal, R., Carroll, B., Sheplak, M., and Cattafesta, L., "A Jet Formation Criterion for Synthetic Jet Actuators," AIAA Paper 2003-0636, Jan. 2003.

[22]Didden, N., "On the Formation of Vortex Rings: Rolling-Up and Production of Circulation," *Journal of Applied Mathematics and Physics*, Vol. 30, Jan. 1979, pp. 101–116.

[23]Utturkar, Y., Mittal, R., Rampunggoon, P., and Cattafesta, L., "Sensitivity of Synthetic Jets to the Design of the Jet Cavity," AIAA Paper 2002-0124, Jan. 2002.

[24]White, F. M., *Viscous Fluid Flow*, McGraw–Hill, Boston, 1991.

[25]Saffman, P. G., *Vortex Dynamics*, Cambridge Univ. Press, Cambridge, England, U.K., 1997.

[26]Pierrehumbert, R. T., "A Family of Steady, Translating Vortex Pairs with Distributed Vorticity," *Journal of Fluid Mechanics*, Vol. 99, No. 1, 1980, pp. 129–144.

[27]Udaykumar, H. S., Mittal, R., and Shyy, W., "Computation of Solid-Liquid Phase Fronts in the Sharp Interface Limit on Fixed Grids," *Journal of Computational Physics*, Vol. 153, No. 2, 1999, pp. 535–574.

[28]Ye, T., Mittal, R., Udaykumar, H. S., and Shyy, W., "An Accurate Cartesian Grid Method for Viscous Incompressible Flows with Complex Immersed Boundaries," *Journal of Computational Physics*, Vol. 156, No. 2, 1999, pp. 209–240.

[29]Udaykumar, H. S., Mittal, R., Rampunggoon, P., and Khanna, A., "A Sharp Interface Cartesian Grid Method for Simulating Flows with Complex Moving Boundaries," *Journal of Computational Physics*, Vol. 174, No. 1, 2001, pp. 345–380.

[30]Kotapati, R. B., and Mittal, R., "Time-Accurate Three-Dimensional Simulations of Synthetic Jets in Quiescent Air," AIAA Paper 2005-0103, Jan. 2005.

[31]Mittal, R., and Rampunggoon, P., "On the Virtual Aeroshaping Effect of Synthetic Jets," *Physics of Fluids*, Vol. 14, No. 4, 2002, pp. 1533–1536.

[32]Loudon, C., and Tordesillas, A., "The Use of the Dimensionless Womersley Number to Characterize the Unsteady Nature of Internal Flow," *Journal of Theoretical Biology*, Vol. 191, No. 1, 1998, pp. 63–78.

[33]Smith, B., Trautman, M., and Glezer, A., "Controlled Interactions of Adjacent Synthetic Jets," AIAA Paper 99-0669, Jan. 1999.

[34]Shuster, J. M., and Smith, D. R., "A Study of the Formation and Scaling of a Synthetic Jet," AIAA Paper 2004-0090, Jan. 2004.

[35]Horowitz, S., Nishida, T., Cattafesta, L., and Sheplak, M., "Characterization of a Compliant-Backplate Helmholtz Resonator for an Electromechanical Acoustic Liner," *International Journal of Aeroacoustics*, Vol. 1, No. 2, 2002, pp. 183–205.

[36]Gallas, Q., Holman, R., Nishida, T., Carroll, B., Sheplak, M., and Cattafesta, L., "Lumped Element Modeling of Piezoelectric-Driven Synthetic Jet Actuators," *AIAA Journal*, Vol. 41, No. 2, 2003, pp. 240–247.

[37]Ingard, U., "On the Theory and Design of Acoustic Resonators," *Journal of the Acoustical Society of America*, Vol. 25, No. 6, 1953, pp. 1037–1061.

K. Ghia
Associate Editor